

ERUPTION DYNAMICS OF THE 114ka TRACHYTE ERUPTION

AT PU‘U WA‘AWA‘A, HAWAI‘I

A THESIS SUBMITTED TO THE UNDERGRADUATE DIVISION OF THE UNIVERSITY
OF HAWAI‘I AT MĀNOA IN PARTIAL FULFILLMENT OF THE REQUIREMENTS OF
THE SENIOR THESIS FOR THE DEGREE OF

BACHELOR OF SCIENCE

IN

GEOLOGY AND GEOPHYSICS

AUGUST 2015

By

Tanis C. Leonhardi

Thesis Advisor(s):

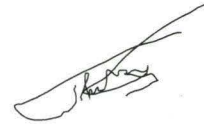
Thomas Shea

Keywords: Pu‘u Wa‘awa‘a; Hawaiian post-shield volcanism; trachyte; magma degassing;
microlites

We certify that we have read this thesis and that, in our opinion, it is satisfactory in scope and quality as a thesis for the degree of Bachelor of Science in Geology and Geophysics.

THESIS ADVISOR(S)

Advisor

A handwritten signature in black ink, appearing to be "J. K. ...", is written over a horizontal line.

ACKNOWLEDGEMENTS

Thank you to my thesis advisor Tom Shea whose passion for pumice and fascination with Pu‘u Wa‘awa‘a and Pu‘u Anahulu helped me gain a new appreciation for volcanology and greatly influenced my decision to pursue volcanology in graduate school. Additionally, thank you to classmate Bryant Servin-Quinonez whose excitement over plagioclase in Hawaiian volcanic rocks helped me find a passion for both minerals and Hawaiian volcanoes. All members of the Hammer Lab are also thanked for their support in completing this thesis and input concerning magmatic processes.

Thank you to Elliot Pearsons (Pu‘u Wa‘awa‘a Forest Preserve) and the Hawaii Experimental Tropical Forest (HEFT) are thanked for their help with in-site access. Special thanks to E. Hellebrand for performing XRF analyses. This thesis has benefited greatly from conversations with T. Giachetti, E. First, and J. Hammer and numerous hours invested by my thesis advisor T. Shea. Research was supported through funding by NSF grant EAR-1250366.

ABSTRACT

Volcanic research in Hawai‘i tends to focus on basaltic compositions as the Hawaiian Islands are made dominantly of basalt. However, amongst all the basalt outcrop four units with evolved compositions. No physical volcanological study has been conducted on one of these highly evolved compositions in the past. One of these outcrops consists of Pu‘u Wa‘awa‘a tephra cone and Pu‘u Anahulu lava flow, collectively called the Wa‘awa‘a Volcanics, both of which are alkaline trachytes. The Wa‘awa‘a Volcanics’ temporal occurrence marking the transition to Post-Shield volcanism at Hualālai combined with the linked tephra cone and lava flow provide a unique opportunity to study eruption dynamics of the transition to post-shield volcanism, the transition between effusive and explosive volcanic activity, and determine whether the two units are co-eval.

To determine the eruption dynamics and magma chamber conditions resulting in the Wa‘awa‘a Volcanics we used a combination of field observations, textural component classifications, density measurements, frequency distribution diagrams, petrography observations, and X-Ray Fluorescence Spectrometry (XRF) chemical analyses. Macro- to micro-scale observations, textural components, and density distributions revealed a Vulcanian eruption style for the formation of Pu‘u Wa‘awa‘a tephra cone. Whole-rock chemical analyses revealed subtle differences between the two units, which combined with field observations of Pu‘u Wa‘awa‘a pumice atop Pu‘u Anahulu lava flow led us to conclude that the units were not co-eval. The results of this study can be used to help understand silicic volcanism in Hawai‘i and increase understanding of monogenetic trachytic volcanism.

TABLE OF CONTENTS

ACKNOWLEDGEMENTS	iii
ABSTRACT	iv
LIST OF TABLES	vii
LIST OF FIGURES	viii
CHAPTER 1. INTRODUCTION	1
1.1. Geologic Background	1
1.2. Literature Summary	6
1.3. Context of this Study	7
CHAPTER 2. METHODS	11
2.1. Sampling	11
2.2. Density Measurements	13
2.3. Textural Observations and Componentry	14
2.4. Petrography	16
2.5. XRF (X-Ray Fluorescence) Spectrometry Techniques	16
CHAPTER 3. RESULTS	17
3.1. Qualitative Results	17
3.1.1. Macroscopic Clast Textures	17
3.1.2. Clast Mineralogy	18
3.1.2a. Clast Mineralogy: Feldspar	18
3.1.2b. Clast Mineralogy: Oxides	21
3.1.2c. Clast Mineralogy: Pyroxene/ Amphibole	22
3.1.3. Vesicle Characteristics	22

3.1.4. Banding Characteristics	25
3.2. Quantitative Results	27
3.2.1. Componentry	27
3.2.2. Density Distributions	29
3.2.3. XRF Whole Rock Compositions	38
CHAPTER 4. DISCUSSION	42
4.1. Accounting for textural diversity through eruption style	42
4.2. Eruption Model for the Wa'awa'a Volcanics	43
4.3. Evolution of the Pu'u Wa'awa'a Magma	49
CHAPTER 5. CONCLUSIONS	57
REFERENCES	59

LIST OF TABLES

Table	Page
3.1 Mineral characteristics observed in each textural component	20
3.2 Vesicle characteristics for each textural component.....	23
3.3 Observed banding types and distinguishing characteristics.....	26
3.4 Bulk rock density mode values and vesicularity for Pu'u Wa'awa'a juvenile clasts by stratigraphic unit	30
3.5 Average bulk rock density values and vesicularity for Pu'u Wa'awa'a pumiceous clasts by stratigraphic unit.....	33
3.6 Average bulk rock density values and vesicularity for Pu'u Wa'awa'a scoriaceous, Sc, clasts by stratigraphic unit.....	34
3.7 Average values of bulk rock density and vesicularity for Pu'u Wa'awa'a microcrystalline, Mc, clasts by stratigraphic unit.....	35
3.8 Average values of bulk rock density and vesicularity for Pu'u Wa'awa'a obsidian, Ob, clasts by stratigraphic unit.....	37
3.9 Whole-rock compositions of selected Pu'u Wa'awa'a clasts and Pu'u Anahulu lava blocks.....	39
4.1 Observed and predicted changes in oxide abundances for fractional crystallization of a feldspar phase.....	52
4.2 Observed changes in oxide wt. % from Pu'u Anahulu to Pu'u Wa'awa'a compositions.....	55

LIST OF FIGURES

Figure	Page
1.1 Map of Hawai'i Island and Hualālai volcano.....	3
1.2 Map of Pu'u Wa'awa'a and Pu'u Anahulu with inferred flow outline 114ka and present.....	4
2.1 Map of Hualālai with marked location of sampling site at Pu'u Wa'awa'a.....	12
2.2 Textural classes identified in this study.....	15
3.1 Photomicrographs showing typical crystal phases of each textural component.....	19
3.2 Photomicrographs of typical vesicle characteristics for each textural component.....	24
3.3 Clast frequency stratigraphic column.....	28
3.4 Density distribution by stratigraphic unit.....	31
3.5 TAS classification for Pu'u Wa'awa'a trachyte clasts and Pu'u Anahulu lava blocks.....	40
3.6 SiO ₂ variation diagrams for bulk rock compositions.....	41
4.1 Conceptual eruption model.....	45
4.2 Summary of fractional crystallization of Pu'u Wa'awa'a magma.....	54

CHAPTER 1.

INTRODUCTION

1.1. GEOLOGIC BACKGROUND

The Hawaiian Islands are located in an intra-plate tectonic setting in the interior of the Pacific Plate and are the product of hotspot volcanism. Hotspot volcanism in the Hawaiian Islands is commonly attributed to the upwelling of a mantle plume of abnormally hot rock that originates at the core-mantle boundary, rises, decompresses, and eventually erupts (Walker, 1990). Gently sloping shield volcanoes gradually grow on the seafloor until they breach sea-level and form the volcanic islands we observe today (MacDonald *et al.*, 1983; Clague, 1987; Walker, 1990). When a volcano is located directly above the Hawaiian hotspot it is in the shield-building stage of a Hawaiian volcano. This stage is distinguished by the highest volumes of magma discharge of all stages and lavas with a tholeiitic composition (MacDonald *et al.*, 1983; Clague, 1987; Moore *et al.*, 1987; Frey *et al.*, 1990; Walker, 1990).

As the volcano moves away from the hotspot, volcanic activity decreases, and magma compositions become more alkalic (MacDonald *et al.*, 1983; Clague, 1987). Distancing from the hotspot cools the oceanic lithosphere beneath the volcano resulting in reduced degrees of partial melting of magmatic source material and more alkali-rich composition. This period of reduced volcanic activity following the shield-building stage, and characterized by alkalic magma compositions, is referred to as the post-shield stage of the life-cycle of a Hawaiian volcano (Clague, 1987; Frey *et al.*, 1990). Magmas erupted during this stage gradually become more silica-rich as the source magma

chamber evolves through fractional crystallization of various mineral phases (Moore *et al.*, 1987; Frey *et al.*, 1990; Cousens *et al.*, 2003). In a few circumstances, alkalic magmas evolve to such a great extent that trachyte lavas may be erupted (MacDonald *et al.*, 1983; Clague, 1987).

Highly evolved lava compositions are uncommon in the Hawaiian Islands with only four documented surface exposures in the main Hawaiian Islands (MacDonald and Katsura, 1964; MacDonald *et al.*, 1983; Sherrod *et al.*, 2007). One of these rare occurrences is a cluster of monogenetic trachyte volcanism referred to as the Wa'awa'a Volcanics located on the NE flank of Hualālai Volcano on the Island of Hawai'i (Figure 1.1) (Clague, 1987; Moore *et al.*, 1987; Sherrod *et al.*, 2007). The Island of Hawai'i has five volcanoes, both active and dormant, one of which, Hualālai Volcano, is noted as being in its post-shield phase due to the presence of the highly evolved trachyte compositions of the Wa'awa'a Volcanics, and more recent alkali lavas (Kauahikaua *et al.*, 2000; Cousens *et al.*, 2003; Shamberger and Hammer, 2006).

The trachytic Wa'awa'a Volcanics are composed of the Pu'u Wa'awa'a tephra cone which has a diameter roughly 1.6 km across and Pu'u Anahulu trachyte lava flow which together constitutes a total eruption volume of $\sim 5.5 \text{ km}^3$ (MacDonald *et al.*, 1983; Clague, 1987; Moore *et al.*, 1987). The Pu'u Anahulu lava flow consists of multiple flow lobes amassing to a total thickness of approximately 275m and extending over 9km away from the Pu'u Wa'awa'a vent (Clague, 1987; Moore *et al.*, 1987; Cousens *et al.*, 2003). Younger lava flows have partially covered the Pu'u Anahulu lava flow but work by Stearns and MacDonald (1946) has resulted in an inferred flow path (Figure 1.2). The covering of Pu'u Anahulu by more recent flows means surface exposures showing that

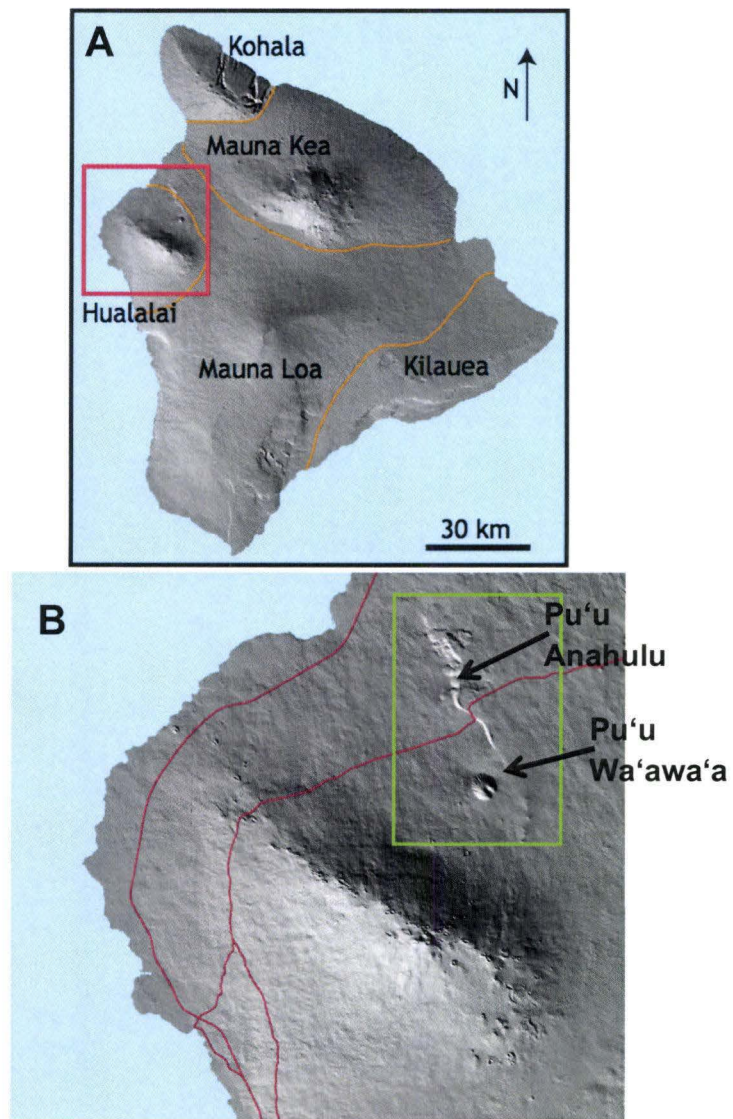


Figure 1.1 – (A) The Island of Hawai'i with Hualālai volcano outlined in orange and labeled with its name. (B) The area outline by the red square is enlarged to better show Pu'u Wa'awa'a Cone and Pu'u Anahulu flow.

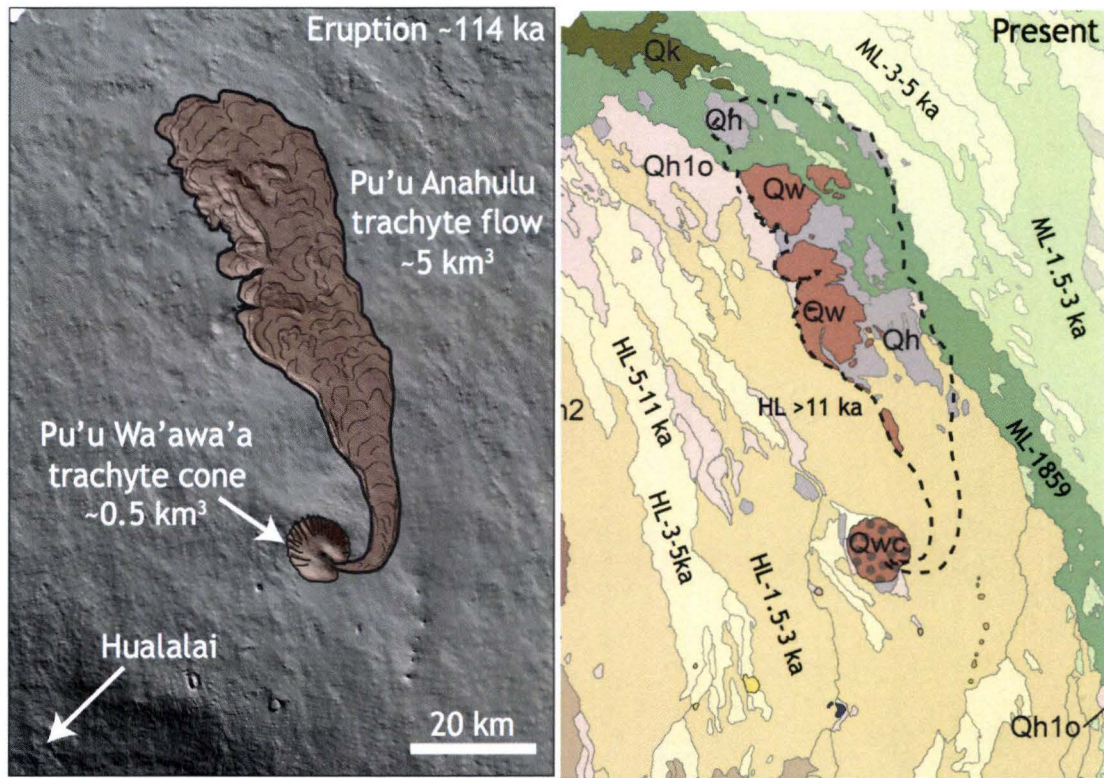


Figure 1.2 – (Left) Inferred outline of Pu'u Anahulu lava flow on a Digital Elevation Model (DEM). Outline inferred from Stearns and MacDonald, 1946. (Right) The Wa'awa'a volcanics are represented by the units starting with Qw. Qw refers to Pu'u Anahulu flow and Qwc refers to Pu'u Wa'awa'a trachyte cone (Map modified from Sherrod *et al.*, 2007).

the Pu‘u Anahulu lava flow in fact originated from the Pu‘u Wa‘awa‘a cone no longer exist (Washington, 1923; Stearns and MacDonald, 1946). The lack of surficial evidence connecting these two units raises the question of whether these features were co-eval (e.g. formed during the same eruption from the same magma source) or whether they formed during two disparate events.

The eruption of the Wa‘awa‘a Volcanics marked the first volcanic activity at Hualālai volcano following an apparent 20ka gap in volcanic activity (Moore *et al.*, 1987; Clague, 1987; Cousens *et al.*, 2003). Recent $^{40}\text{Ar}/^{39}\text{Ar}$ dating performed by Cousens *et al.* (2003) has placed the time of formation of the Pu‘u Anahulu lava flow at 114ka. The Wa‘awa‘a Volcanics marked a dramatic change in composition from tholeiitic basalt to highly evolved alkalic compositions, and thus mark the transition from shield-building to post-shield volcanism at Hualālai volcano (Clague, 1987; MacDonald *et al.*, 1983; Cousens *et al.*, 2003; Shamberger and Hammer, 2006).

Trachyte lava flows and monogenetic tephra cones are relatively uncommon internationally and exceptionally rare in Hawaiian volcanism (MacDonald and Katsura, 1964; MacDonald *et al.*, 1983; Spengler and Garcia, 1988; Wolf *et al.*, 1997; Sherrod *et al.*, 2007). Aside from the Wa‘awa‘a Volcanics there are three other Hawaiian eruptions involving highly-evolved magmas reported in the Hawaiian Islands: Mauna Kuwale rhyodacite flow, Oahu; trachyte domes, West Maui; Hawi flows and domes, Kohala (MacDonald *et al.*, 1983; Sherrod *et al.*, 2007). Due to the aforementioned lack of deposits with such evolved compositions in the Hawaiian Islands, the Wa‘awa‘a Volcanics provide a unique opportunity to try and understand the transition from shield-

building to post-shield volcanism in the Hawaiian Islands and the eruption dynamics associated with trachyte volcanism.

1.2. LITERATURE SUMMARY

In 1904, Whitman Cross first documented the occurrence of the Wa‘awa‘a complex on the flank of Hualālai (Cross, 1904). His observations match those of later reports and he concluded that at least three different eruption products were present in eruption deposits: pumice, obsidian, and a very dark-colored, dense clast, which resembled basalt. Subsequent inquiries by H.S. Washington in 1923 and Stearns and MacDonald in 1946 all document the presence of multiple flow units of holocrystalline trachytic material separated by layers of pumice. Additionally, the different types of componentry identified at Pu‘u Wa‘awa‘a cone in these studies included pumiceous clasts, black glassy obsidian clasts, dark gray holocrystalline clasts, and dull yellowish clasts.

As previously mentioned, the Pu‘u Wa‘awa‘a cone is thought to mark the transition from the shield building stage to the post shield stage of Hualālai volcano (Moore *et al.*, 1987; Clague, 1987; Frey *et al.*, 1990). Two main theories have previously been proposed to explain the formation of trachyte magma reservoirs at Hualālai. The first theory suggests that they formed following the termination of shield-building volcanic activity at Hualālai volcano, which would allow for ~20k years for the magma to evolve from a tholeiitic basalt to a trachyte composition (Clague, 1987; Cousens *et al.*, 2003). The second theory states that the trachyte reservoir started forming during the end of shield-building activity at Hualālai volcano (Cousens *et al.*, 2003).

While there exists multiple hypotheses as to when the trachyte magma chamber began to form, it is generally believe that evolution of the magma chamber occurred due to fractional crystallization of an alkali basalt parental magma (Clague, 1987; Moore *et al.*, 1987; Cousens *et al.*, 2003; Shamberger and Hammer, 2006). Alkali basalts are usually considered transitional compositions in Hawaiian volcanism (Clague, 1987; MacDonald *et al.*, 1983). Initial bulk rock compositions from a study conducted by Cousens *et al.*, (2003) shows that the Pu‘u Wa‘awa‘a and Pu‘u Anahulu samples are identical in regards to isotopic composition. However, it should be noted that their major and trace element compositions show subtle differences between samples from the two units.

In addition to the diverse range of components preserved in the volcanic deposits at Pu‘u Wa‘awa‘a and Pu‘u Anahulu, more recently erupted lava flows from Hualālai in 1800-1801 included crustal xenoliths. Previous studies of these xenoliths have found that they contain cumulate material (Clague and Bohrsen, 1991; Cousens *et al.*, 2003; Shamberger and Hammer, 2006). The cumulate material in these xenoliths formed by fractional crystallization of alkali basalt, resulting in a trachytic magma composition (Clague, 1987; Bohrsen and Clague, 1988; Clague and Bohrsen, 1991; Cousens *et al.*, 2003; Shamberger and Hammer, 2006).

1.3. CONTEXT OF THIS STUDY

Discussed below are several important questions this study aims to answer.

What were the magmatic conditions leading to the eruption of the 114ka Pu‘u Wa‘awa‘a trachyte eruption?

While previous literature has recorded observations of different lithologies contained in the Pu‘u Wa‘awa‘a cone (Cross, 1904; Washington, 1923; Stearns and MacDonald, 1946; MacDonald *et al.* 1983; Moore *et al.* 1987; Clague, 1987) no physical volcanological study has been performed with the intent to understand the dynamics driving the eruption of the Wa‘awa‘a Volcanics. Since much of the eruption deposits of the Wa‘awa‘a Volcanics have been covered by more recent flows, grain size analysis of fallout cannot be conducted, and inferences about eruption dynamics must be made through exposures at Pu‘u Wa‘awa‘a cone and Pu‘u Anahulu terraces. We will be using a combination of textural observations, both at the macroscopic and microscopic scale, field-observations, and bulk rock XRF analyses to determine what the magmatic conditions were that ultimately led to the eruption of the Pu‘u Wa‘awa‘a trachyte cone and the Pu‘u Anahulu lava flow.

How do we account for the variety of textural components within each deposit?

The presence of obsidian alongside pumice, microcrystalline material, and scoriaceous material is unique in Hawai‘i and an eruption model must be developed which can produce the textural variety observed in each stratigraphic unit. We will evaluate the possibility that these components are (1) inherent to the magma reservoir (2) the result of conduit processes or (3) the result of post-fragmentation processes.

Were Pu‘u Wa‘awa‘a cone and Pu‘u Anahulu lava flow co-eval?

Research over the past couple decades has started to reveal a change in volcanic eruption style from explosive to effusive during a single episode of volcanic activity is strongly linked to the extent of magmatic degassing (e.g. Eichelberger *et al.*, 1986; Jaupart and Allegre, 1991; Woods and Koyaguchi, 1995; Hammer *et al.*, 1999; Barmin *et*

al., 2002; Gonnermann and Manga, 2007; Degruyter *et al.*, 2012). Determining the processes governing this transition are an area of active research as understanding those processes increases understanding of why a volcano erupts explosively and what controls the explosivity of a given eruption (Eichelberger *et al.*, 1986; Woods and Koyaguchi, 1995; Gonnermann and Manga, 2003). We will use a combination of mineralogy, bulk rock XRF analyses and textural observations to determine if these units are co-eval.

What can our results tell us about eruption dynamics of Hawaiian volcanoes during their transition to Post-Shield volcanism?

The transition to the post-shield stage of Hawaiian volcanoes remains poorly understood. The Island of Hawai‘i currently is home to three post-shield stage volcanoes: Kohala, Mauna Kea, and Hualālai, but Hualālai is the only volcano of these three that has erupted in historic times (Bohrson and Clague, 1988; Walker, 1990). Hualālai provides the unique opportunity to study the eruption products from the transition to the post-shield stage and place these eruptions in the context of more recent eruptions. As Hualālai has erupted in historic times and currently has people residing on its flanks, understanding the dynamics of the monogenetic eruption of the Wa‘awa‘a Volcanics is not only useful in determining sub-surface geological structures, but also in determining potential hazards associated with different eruption styles (Walker, 1990).

By understanding the eruption dynamics of the Wa‘awa‘a Volcanics we are hoping to help add to the knowledge of post-shield volcanism with highly evolved compositions and associated hazards and tie the obtained data for the Wa‘awa‘a Volcanics into our understanding of Hawaiian volcanism.

To provide a new view on eruption dynamics we used a combination of volcanological, petrographic, and geochemical techniques in the first in-depth physical volcanology study of highly-evolved post-shield volcanics in the Hawaiian Islands. Field samples were collected by Thomas Shea at the main quarry at Pu‘u Wa‘awa‘a cone and along Pu‘u Anahulu lava flow. We used textural observations to determine distinct textural components present in all volcanic units and performed density measurements on all clasts to obtain density distributions for each stratigraphic unit sampled. Selected clasts from each unit were cut and made into thin sections for microscopic textural observations. We also performed additional bulk rock analyses on samples from both Pu‘u Wa‘awa‘a and Pu‘u Anahulu to confirm that our results showed subtle variations in major element abundances between sampled flow and cone clasts.

Using the obtained data we evaluated our results in the context of explosive eruption styles to determine how Pu‘u Wa‘awa‘a cone was erupted and develop a conceptual eruption model. Our results were also evaluated in the context of Hawaiian volcanism to understand the magma chamber evolution dynamics resulting in the formation of Wa‘awa‘a Volcanics and increase understanding of the transition of a Hawaiian volcano to the post-shield stage. Finally, we evaluated our results in the context of the explosive to effusive transition by determining if the two units were co-eval.

CHAPTER 2.

METHODS

2.1. SAMPLING

The Wa‘awa‘a Volcanics posed a unique challenge for conducting field-work. Because fall deposits from the Wa‘awa‘a eruption have been covered by more recent lava flows from Mauna Loa and Hualālai (Figure 1.2), only the most proximal deposits were available for sampling. The volcanic stratigraphy showed that significant syn-eruptive remobilization of deposits had occurred, which was observable through discontinuous stratigraphic units, ‘duplexing’ of numerous beds, and ‘lensing’. Of these units, six relatively continuous, thick stratigraphic ‘packets’ were distinguished on the basis that they could be recognized at different outcrops at the cone. Subunits within these 6 ‘packets’ were generally enriched in darker clasts at the base and progressively richer in lighter material at the top, with a general reverse-grading.

Representative clasts from each subunit of the 6 main packets were collected in the summer of 2013. Sampling was conducted at the existing quarry on the NE side of the tephra cone (Figure 2.1). Around 100 clasts were sampled within defined of diameter 10-32mm for density measurements. Only well-preserved clasts were analyzed in an attempt to remove potential affects due to secondary alteration. Sampling was performed horizontally within a narrow portion of the stratigraphic unit. These sampling methods are commonly used when collecting pyroclastic material (Houghton and Wilson, 1989; Gurioli *et al.*, 2005).

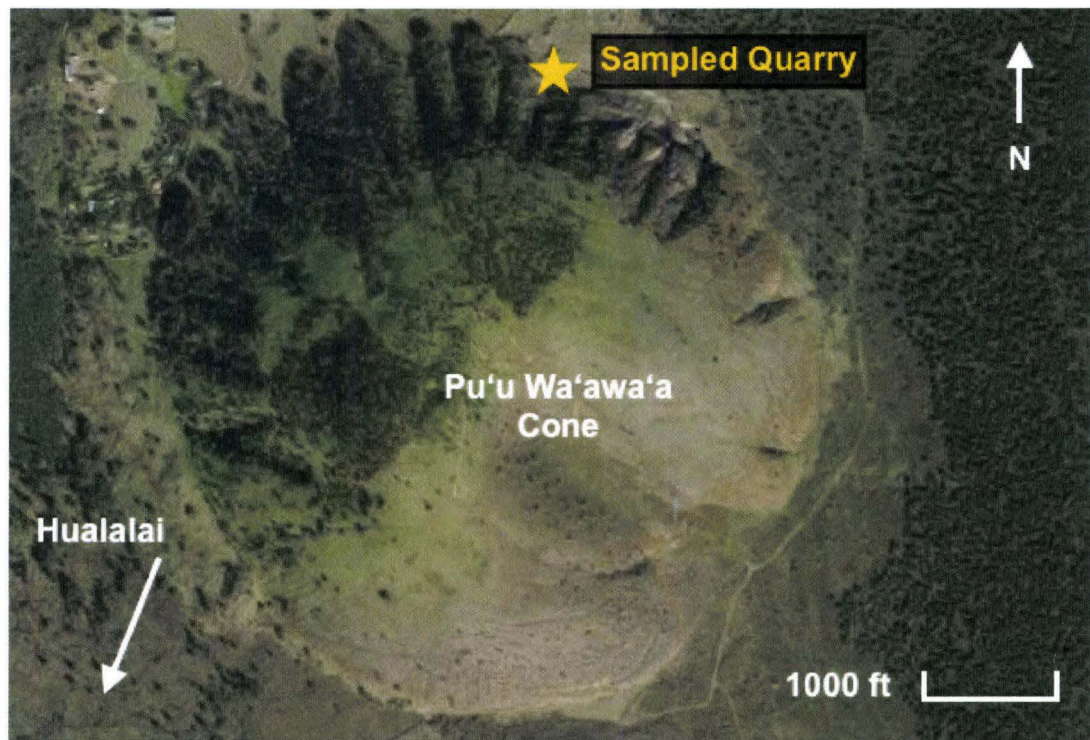


Figure 2.1 – Location of the sampled quarry relative to Pu'u Wa'awa'a tephra cone and Hualalai summit.

2.2. DENSITY MEASUREMENTS

Collected samples were cleaned in distilled water using an ultrasonic bath in order to remove alteration, dirt, and ash and then dried at approximately 75°C for 24h. Clasts of diameter 10-32mm were arranged in order of decreasing size and numbered from 1-100, with 1 representing the largest clast and 100 the smallest. In one sample, only 84 clasts were of the desired size and in a few other units, up to 135 clasts were ranked in order to fill gaps in the density distributions.

Clasts were then weighed in air, wrapped in parafilm wax, and submerged and weighed in water. Archimede's principle was used to determine the density of clasts by accounting for the weight of the parafilm wax and the weight of the clast in air and in water in the following equation where ρ_{film} is the density of one square of the parafilm wax used to wrap each clast and f is the fraction of a parafilm square used to wrap the clast.

$$\rho_{clast} = \rho_{water} \left(\frac{w_{clast}^{air}}{w_{clast}^{air} - w_{clast+film}^{water} - \rho_{film}f} \right)$$

In the above equation ρ_{clast} represents the density of the clast being measured, ρ_{water} is the density of water at 25°C, w_{clast}^{air} is the mass of the clast in air, $w_{clast+film}^{air}$ is the mass (in air) of the clast wrapped in parafilm, and f is the amount of parafilm used represented as a fraction of one square.

A ballast was submerged in water, tared to zero, and then the clast being measured was placed in the ballast and submerged in water. Clasts with a density higher than that of water (at 25°C, 0.997 g/cm³) recorded positive weights and clasts that floated recorded negative weights. The dense rock equivalent (DRE) of the magma was

determined to be 2.56 g/cm³, and was used in the following equation to determine porosity, ϕ , or vesicularity ($\phi \times 100$) for each clast (Shea *et al.*, 2010).

$$\phi = \frac{\rho_{DRE} - \rho_{clast}}{\rho_{DRE}}$$

2.3. TEXTURAL OBSERVATIONS AND COMPONENTRY

Sampled clasts were classified based on physical characteristics into four distinct textural end-members. While each end-member component was characterized by a distinct set of features, clasts were often gradational between the end-members and/or exhibited banding of the different components. A clast composed with >50% of one component was classified as being a member of that textural class.

We distinguished four main textural classes based on macroscopic observations such as color, surface texture, banding, luster, and vesicle morphology (Figure 2.2). The following four end-members lithologies were determined, (1) highly vesicular, light colored **pumiceous clasts**; (2) highly vesicular, dark-colored **scoriaceous clasts**; (3) vesicle-poor, dark colored, glassy clasts, which we called **obsidian** and (4) vesicle-poor, dark colored **microcrystalline clasts** with a dull or earth luster. The samples from the Pu‘u Anahulu were vesicle-poor, light colored with darker bands, and crystal-rich and constituted a fifth textural component (Figure 2.2E).

Following the distinguishing of textural components from Pu‘u Wa‘awa‘a tephra cone, an expedition to Pu‘u Anahulu lava flow was performed by Thomas Shea to see if there was any textural evidence linking the two units. Pumice on top of the Pu‘u Anahulu lava flow was determined to belong to Pu‘u Wa‘awa‘a.

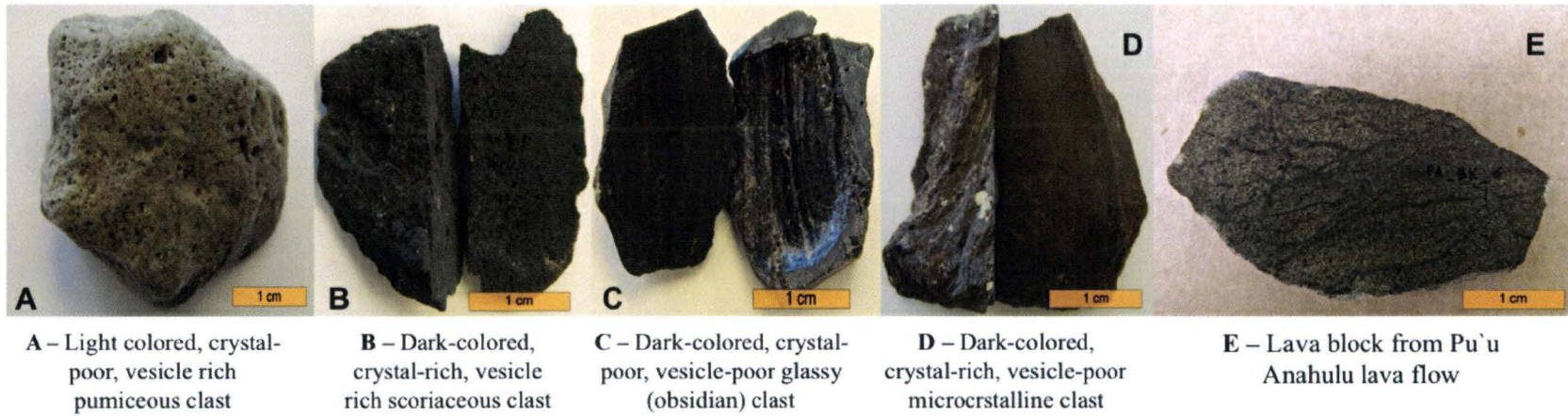


Figure 2.2 – The five textural end-member components identified in Pu'u Wa'awa'a deposits.

2.4. PETROGRAPHY

Density distributions for all clasts from each sample were produced as histograms with 0.1 g/cm^3 bin increments. From each histogram, 5-7 clasts were chosen for petrographic observations. The clasts with the highest and lowest densities were chosen, as well as 1-3 clasts representative of each density mode (Shea *et al.*, 2010). This selection resulted in at least one clast of each textural component per sample being selected for further petrographic studies. Slabs were made manually from selected clasts cut perpendicular to the plane of flow banding, if present, or other internal features of interest. The slabs were then used to make 75 thin sections, 66 of Pu'u Wa'awa'a clasts and 9 of Pu'u Anahulu lava blocks.

2.5. XRF (X-RAY FLUORESCENCE) SPECTROMETRY TECHNIQUES

Major element compositions were determined for 9 samples from the Pu'u Anahulu flow and 9 samples from the Pu'u Wa'awa'a cone. At least one clast representing each textural component was selected for bulk analyses in order to make sure all clasts were represented in the analyses. Clasts selected for analyses had minimal to no surface alteration, and if surface alteration was present, a rock saw was used to remove it. Samples selected were crushed using a hydraulic press, cleaned using distilled water in an ultrasonic bath, dried at 100°C for 12 hours and then powdered using a WC (Tungsten-Carbide) sawmill. Major-element oxides were determined using X-ray fluorescence (XRF) spectrometry. Analyses were conducted on the University of Hawai'i' Siemens 303AS fully automated, wavelength dispersive, XRF spectrometer.

CHAPTER 3.

RESULTS

3.1. QUALITATIVE RESULTS

3.1.1. Macroscopic Clast Textures

Distinct textural characteristics of each textural class can be found in Figures 2.2, 3.1 and 3.2 and Tables 3.1-3.3. Crystal contents were determined relatively between textural classes.

Pumiceous clasts were generally rounded, light brown to light gray in color, had a high vesicularity, and many contained fragments of darker material, typically aggregates of holocrystalline material (Figure 2.2A). Banding was common in pumiceous clasts between lighter and darker colored pumice as well as between pumiceous and scoriaceous material. Vesicles tended to be large and rounded or small and rounded and were the largest of any class. Some pumiceous clasts contained very elongate vesicles.

Scoriaceous clasts were dark gray to black in color, contained a smaller observable percentage of vesicles on the macro-scale than pumiceous clasts and ranged from a dull to glassy surface (Figure 2.2B). Banding between scoriaceous material and pumiceous material was common as well as banding between scoriaceous and microcrystalline material. Vesicles were moderately high in abundance, were smaller than in the pumiceous clasts and tended to have angular outlines controlled by surrounding microlites.

Crystal-rich, vesicle-poor microcrystalline clasts had a dark purple to black color and typically had smooth surfaces with signs of alteration and a dull luster (Figure 2.2C). Crystal contents were the highest in these clasts within the four Pu'u Wa'awa'a textural

classes and vesicle contents were lower than vesicularities for the pumiceous and scoriaceous components.

Crystal-poor, vesicle-poor obsidian, were typically black to very dark green in color and usually occurred banded with another textural component (Figure 2.2D). Vesicles and crystals were not observable on a macroscopic scale.

While pumiceous, scoriaceous, microcrystalline, and obsidian clasts were the four dominant textural components in the Pu'u Wa'awa'a deposits, most clasts were gradational between these end-members. Additionally, many clasts showed banding between two or more different textural classes while other clasts appeared to be amalgamations of different components held together by ash. These clasts were rare and did not represent a distinct textural class in the Pu'u Wa'awa'a deposits, we referred to these clasts as 'volcanic breccia'.

3.1.2. Clast Mineralogy

The main phases observed both in the Pu'u Wa'awa'a clasts and the Pu'u Anahulu lava blocks were feldspar and oxides. Pu'u Anahulu also contained amphibole or pyroxene as an interstitial groundmass phase, but this phase was uncommon in Pu'u Wa'awa'a clasts. A summary of the micro-structures observed for crystal phases within each textural component and is given in Table 3.1 and Figure 3.1 shows typical mineralogy for each textural class.

3.1.2a. Clast Mineralogy: Feldspar

Pumiceous clasts had the lowest mineral abundances of all textural classes. If crystals were present, they were present as randomly oriented feldspar laths. Occasionally, aggregates of holocrystalline material dominated by small feldspar crystals were found in bands of vesicles in pumiceous clasts. Scoriaceous clasts had higher

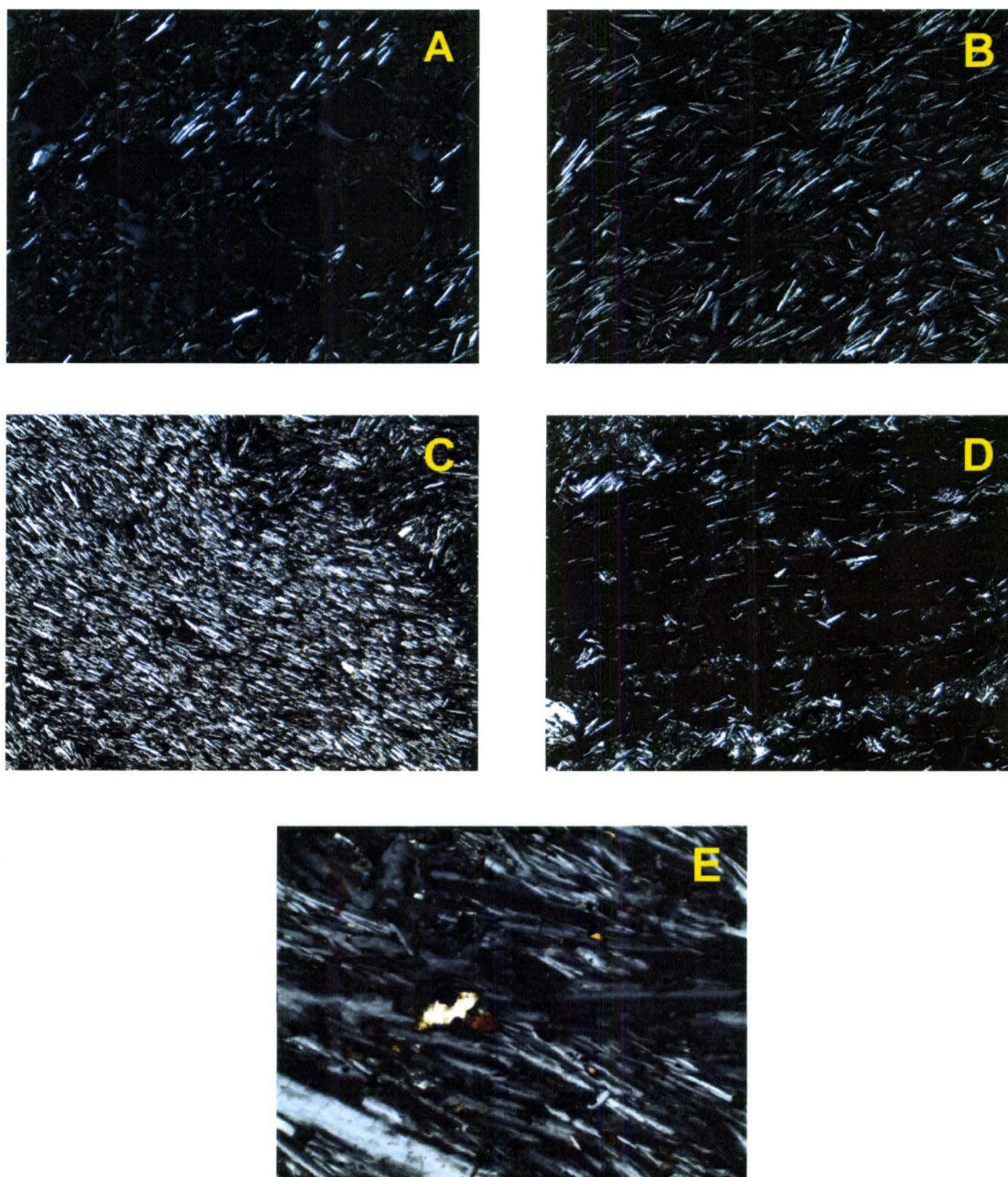


Figure 3.1 – (A) Pumiceous clast in cross polarized light the scarcity of observed feldspar microlites. (B) Scoriaceous clast showing moderately high feldspar abundance. (C) Microcrystalline clast showing very high crystal content and feldspar lath alignment. (D) Obsidian clast showing bands of feldspar crystals aligned parallel to the plane of flow. (E) Pu'u Anahulu lava block showing very large feldspar crystals and small crystals with some alignment and interstitial pyroxene. All photomicrographs are in cross polarized light (XPL), 5x magnification, field of view is 3mm.

Table 3.1 – Mineral characteristics observed in each textural component.

Dominant Textural Type	Feldspar	Oxides	Pyroxene/ Amphibole	Phenocrysts Present?	Aggregates
Pumiceous	Low abundance, as small randomly oriented laths	-	-	No	Aggregates of holocrystalline material sometimes present in vesicle bands
Scoriaceous	Moderate abundance, stellate to randomly oriented thin feldspar laths	Present in trace amounts, typically very small with rounded edges	-	No	Aggregates of holocrystalline material sometimes present in vesicle bands
Microcrystalline	High abundance, occurred as larger crystals with well-defined Carlsbad twinning and spongy rings, in addition to smaller microlite crystals aligned elongate parallel to the plane of flow	Present in minor amounts, sometimes rounded, but typically subhedral to euhedral	Fragments of fractured crystals were identified by distinct cleavage, light green color, and high positive relief Present in units 351, 651, 652	Yes, infrequently: - Feldspar - Oxides	No
Obsidian	Low abundance, thin feldspar crystal aligned parallel to plane of flow	Randomly interspersed	-	No	No
Pu'u Anahulu	High abundance, occurred as larger crystals with well-defined Carlsbad twinning and spongy rings some laths were over 2mm in length	Relatively high abundance and occurred as subhedral to euhedral large crystals	Present as an interstitial groundmass phase and occasionally as cluster of very small micro-phenocrysts	Yes, commonly: -Feldspar -Oxides	No

crystal contents than pumiceous clasts, and crystals tended to be slightly larger in size. Additionally, feldspar laths were larger than in pumiceous clasts and appear to increase in size from stratigraphic top to base (e.g. the largest feldspar laths were in unit 652 while the smallest laths were in unit 151). Feldspar crystals did not exhibit an overall preferred orientation and sometimes had a stellate habit around vesicles.

Of the four textural classes from Pu‘u Wa‘awa‘a cone, microcrystalline clasts had the highest crystal content. The clasts were dominated by relatively large feldspar laths exhibiting Carlsbad twinning. Laths typically aligned with elongate edges parallel to elongate edges of other feldspar laths. In the majority of clasts, there were a small number of larger feldspar clasts with well-developed Carlsbad twinning and spongy rims, while the rest of the laths were smaller and were variably twinned. Obsidian clasts tended to contain random feldspar crystals oriented length parallel to banding boundaries between obsidian and microcrystalline material.

In banded clasts, feldspar laths showed the characteristics just described for the corresponding banding component. Additionally, feldspar crystals present along the contact between the banded components tended to align parallel to the plane of contact.

3.1.2b. Clast Mineralogy: Oxides

Oxides were not observed in pumiceous clasts, but were present in trace amounts in the other textural end members and typically had rounded subhedral corners to euhedral corners. Crystals at the stratigraphic base tended to be more rounded while crystals at the top units tended to be euhedral. In microcrystalline clasts, oxides were present in minor amounts and were larger than oxides present in the scoriaceous clasts. Crystals were subhedral to euhedral and units 651 and 652 contained one and two

phenocrysts respectively. Additionally, a few oxides were randomly dispersed throughout obsidian samples.

In the Pu‘u Anahulu lava blocks, oxides were large, sometimes up to 1mm x 1mm, and were more abundant than any of the samples from Pu‘u Wa‘awa‘a. These oxides were well formed, with subhedral to euhedral morphologies and occurred both as phenocryst and microphenocryst phases.

3.1.2c. Clast Mineralogy: Pyroxene/Amphibole

Microcrystalline clasts were the only clasts that contained pyroxene and amphibole, and only units 351, 651 and 652 contained this phase at all. When present, crystals were fractured but displayed distinct cleavage and high positive relief. The Pu‘u Anahulu lava blocks had relatively high abundances of pyroxene and amphibole. These were present as interstitial, groundmass phases, and occasionally as small clusters of euhedral crystals or as larger fractured crystals.

3.1.3. Vesicle Characteristics

Vesicle characteristics differed between textural classes and varied in abundance, size, and morphology throughout the stratigraphic units. Table 3.2 provides a summary of observed vesicle characteristics by component. Figure 3.2 contains photomicrographs of commonly observed vesicle characteristics for each textural class.

Vesicles in pumiceous clasts were rounded and relatively large compared to vesicles in other textural classes. Typical clasts contained larger vesicles sometimes with diameters larger than the field of view for minimum, 5x magnification, corresponding to 5mm. Sometimes vesicles appeared squished and some vesicles coalesced. These larger squished vesicles were separated by matrix glass populated by smaller rounded vesicles (Figure 3.2A).

Table 3.2 – Vesicle characteristics for each textural component.

Dominant Textural Component	Relative Abundance	Relative Size	Shape
Pumiceous	High	(1) Very large, with diameters up to >5mm (2) Small, fills in spaces between larger vesicles	(1) Rounded and slightly elongate, sometimes coalesced (2) Rounded, slightly elongate
Scoriaceous	Moderate to High	Moderate in size between small and large vesicles in pumiceous clasts	Sharp, angular edges, pointed corners, morphology controlled by crystal orientations
Microcrystalline	Low	(1) Small individual vesicles (2) Chains of moderately sized vesicles	(1) very irregular in shape, collapsed walls (2) rounded to pinched, but not deflated
Obsidian	Very Low	Very small	Spherical
Pu'u Anahulu	Very Low	Very small	Irregular shape and highly sheared

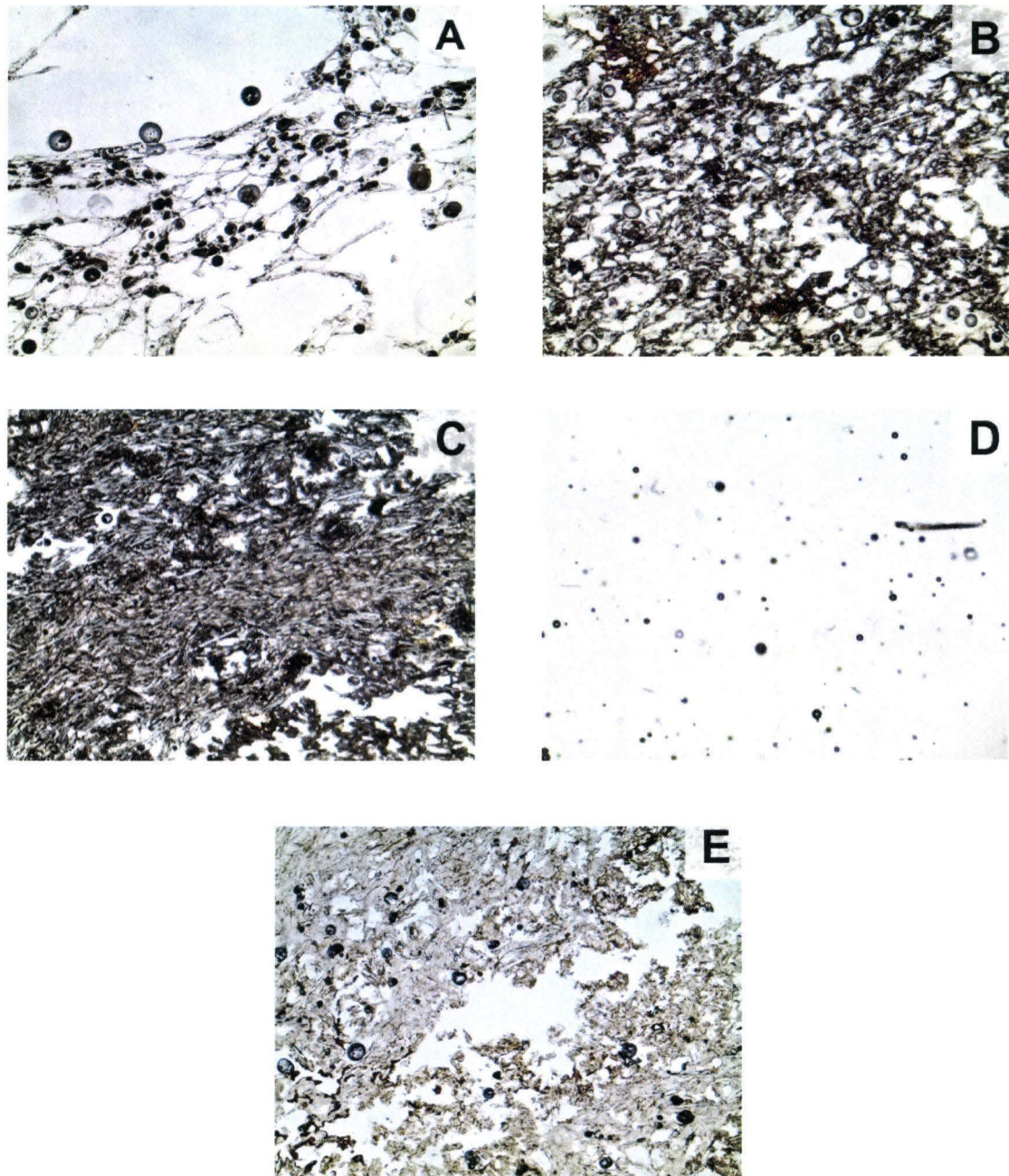


Figure 3.2 – (A) Pumiceous clast showing the two common vesicle sizes of this textural class. (B) Scoriaceous clast showing reduced vesicle size and a more irregular and pinched morphology than pumiceous clasts. (C) Microcrystalline clasts showing lack of vesicles and a chain of vesicles commonly observed in this textural class. (D) Obsidian clast showing the presence of very small spherical vesicle (plane polarized light (PPL), 20x magnification, field of view is 0.3mm). (E) Pu'u Anahulu lava block showing a lack of vesicles except in the formation of chains of irregular vesicles. All photomicrographs are PPL, 5x magnification, and the field of view is 3mm unless otherwise noted.

Vesicles in scoriaceous clasts were less abundant than in pumiceous clasts, as well as smaller, but more abundant than in microcrystalline clasts. Vesicles had more angular edges with more irregular morphologies and crystals often occurred elongate parallel to the long edge of vesicles (Figure 3.2B).

In the microcrystalline clasts, vesicles were small and highly irregular in morphology and their overall shape appeared to be dictated by surrounding crystals protruding on vesicle walls. Vesicles rarely occurred independently, instead they typically formed continuous chains of vesicles that persisted across the expanse of the thin section (Figure 3.2C). When present in obsidian clasts, vesicles were very small and spherical (Figure 3.2D). In the Pu'u Anahulu lava blocks vesicles were irregular and pinched just like the vesicles observed in the microcrystalline clasts (Figure 3.2E).

3.1.4. Banding Characteristics

Flow banding occurred between different textural classes and was characterized by a combination of micro-scale and macro-scale features. A summary of the observed types of banding, the banding types differentiating characteristics, and their corresponding physical properties are given in Table 3.3.

When flow banding was present in pumiceous clasts, bands were typically scoriaceous material. Banding varied from single to multiple occurrences and was wavy to planar and continuous throughout the thin section. Banding in these clasts was relatively planar and band boundaries were marked by differences in vesicle characteristics and crystal content. In a number of clasts, banding between light and dark pumice was also observed. The two pumices were almost identical except the darker

Table 3.3 – Observed banding types and distinguishing characteristics.

Banding Type	Differentiating Characteristics	Macro-Structures	Micro-Structures
Pumiceous - Scoriaceous	Vesicle sizes and shapes, crystal content, color	Observable as bands of light material and dark material with a lower vesicularity	Boundaries between components are convolute and not well defined
Light – Dark Pumice	Crystal content, color	Similar vesicularity between convolute bands of light and dark pumice	Boundaries were diffuse and lacked definitive edges
Scoriaceous-Microcrystalline	Vesicle size, shape, and abundance, crystal alignment	Not easily discernible by hand	Typically boundaries were defined by alignment of feldspar laths and vesicle morphology
Microcrystalline-Obsidian	Crystal content, vesicle size, shape, surface luster	Microcrystalline material typically had a dull surface, obsidian a glassy surface	Edges between bands ranged from distinct to gradational by crystal content
Microcrystalline-Microcrystalline	Crystal alignment	Trachyte texture results in scattering of light from different crystal faces, appears to have a 'sheen'	Feldspar laths within the same flow bands are aligned length parallel to each other and parallel to the plane of flow

pumice tended to have slightly higher crystal content when observed in thin section.

Bands in scoriaceous clasts were typically composed of pumiceous material. In units 651

and 652, banding between microcrystalline and scoriaceous material was also present.

Unlike in pumiceous clasts, multiple banding was common and developed into highly convolute structures.

Flow banding in microcrystalline clasts tended to be between microcrystalline material and glassy, obsidian, material or between bands of feldspar crystals aligned in different directions. Additionally, some of the microcrystalline clasts from lower stratigraphic units contained multiple convolute bands of scoriaceous material. Obsidian typically occurred as thin continuous bands in microcrystalline material. Within obsidian clasts, the only flow banding present was between bands of feldspar crystals with different orientations.

3.2. QUANTITATIVE RESULTS

3.2.1. Componentry

All clasts for each subunit were classified into a representative textural class based on Figure 2.2. Frequencies of each textural component were then counted for each stratigraphic unit, calculated as a percent of the total number of clasts sampled, and were used to compile a diagram of clast componentry versus stratigraphic position (Figure 3.3).

In general, pumiceous clasts were the most abundant clast in each stratigraphic unit. An overall trend is that the fraction of high vesicularity clasts increases with time and lower vesicularity clasts tend to decrease in abundance. Note that there is a sharp drop in the abundance of low vesicularity clasts in units 551 and 251.

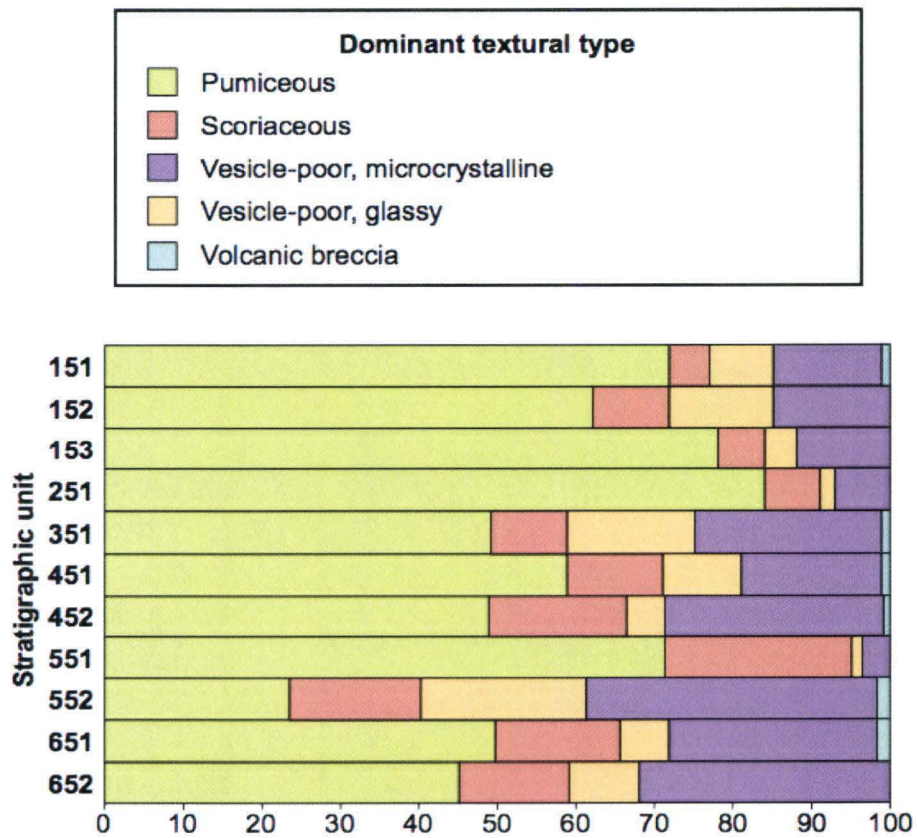


Figure 3.3 – Clast componentry frequency as a function of stratigraphic position.

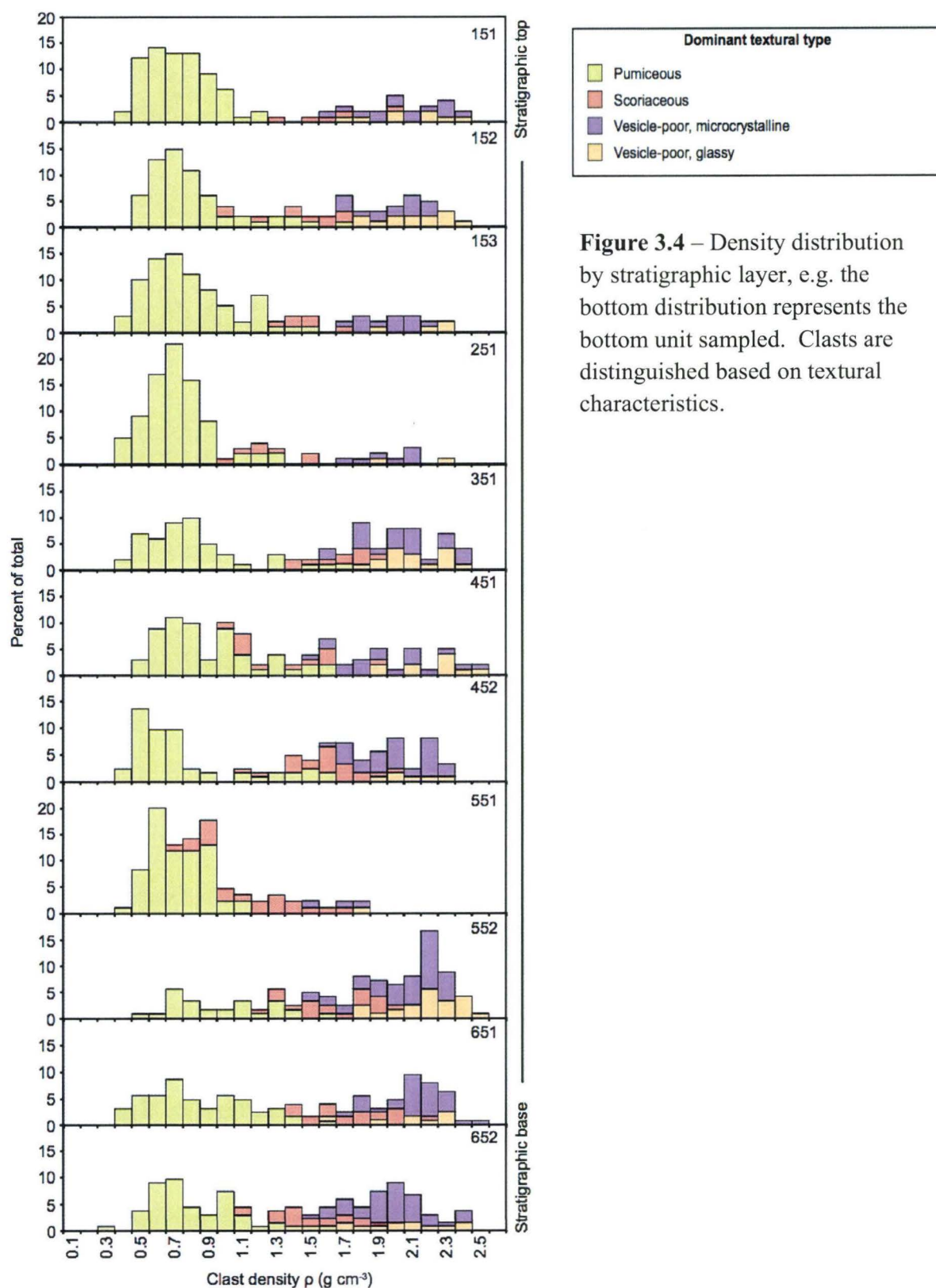
3.2.2. Density Distributions

Density averages were not representative of the density of the clasts sampled due to their textural variety, thus we chose to present the density values for the low, intermediate (sometimes), and high-density modes (Table 3.4). Density data are thus better represented as distributions for each unit of the stratigraphic column (Figure 3.4). The high-density components in each layer tended to correspond with the vesicle-poor, dark-colored microcrystalline and obsidian clasts. Pumiceous clasts overall have the lowest density values, while scoriaceous clasts tend to be gradational in density value between the densities obtained for pumiceous clasts and that obtained for microcrystalline clasts.

Importantly, most stratigraphic units show bimodal density distributions. For most layers, there is a lower density mode populated by the pumiceous clasts and a higher density mode representing the lower vesicularity clasts, predominantly the obsidian and microcrystalline clasts. Scoriaceous clasts tend to be gradational between the pumiceous and high-density modes and sometimes formed a third, intermediate, mode. To see how the density value of each component changed between stratigraphic units we calculated the mean and range for density and vesicularity of each clast by stratigraphic unit (Tables 3.5-3.8). It is important to note the bimodal nature of the sampled units did not carry over to density distributions by textural component. Each textural component had a unimodal density distribution across the sampled units.

Table 3.4 – Bulk rock density values for density distribution modes and average vesicularity for Pu‘u Wa‘awa‘a juvenile clasts by stratigraphic unit.

Sample	<i>n</i>	Low mode ρ (10^3 kg m^{-3})	Int. mode ρ (10^3 kg m^{-3})	Hide mode ρ (10^3 kg m^{-3})	Average Vesicularity (% vol.)	σ (% vol.)	Vesicularity Range
P_151	100	0.65	-	2.05	52.85	23.24	9.16 - 86.12
P_152	100	0.75	1.75	2.15	47.84	23.63	8.24 - 83.54
P_153	100	0.75	-	2.05	57.04	20.12	11.10 - 86.93
P_251	100	0.75	-	2.15	65.14	16.35	13.35 - 87.23
P_351	100	0.85	1.85	2.15	38.90	25.38	6.70 - 86.29
P_451	100	0.75	1.65	2.15	44.34	22.59	3.67 - 84.16
P_452	125	0.55	-	2.05	43.55	24.68	10.41 - 85.87
P_551	84	0.65	-	-	66.77	12.62	30.13 - 85.33
P_552	125	0.75	-	2.25	27.92	20.27	5.78 - 80.87
P_651	125	0.75	-	2.15	38.67	24.98	5.54 - 85.92
P_652	135	0.75	-	2.05	36.79	22.66	7.70 - 88.74



Pumiceous clasts tend to have an average density value in the range of 0.64-0.88 g/cm³ across all units and a mean vesicularity value in the range of 62.93-73.79% (Table 3.5). The mean density range for pumiceous clasts encompasses the low density mode value range across all units (Table 3.4), thus showing that pumiceous clasts represent the low density mode. Note that the density values for the clasts tend to be highest when pumiceous clasts have relatively high overall clast abundances. That is, the modes of low-density clasts are correlated with their abundance. A similar trend occurs for scoriaceous clasts (Table 3.6).

Scoriaceous clasts have a higher range of average density values, 1.05-1.60 g/cm³ compared to the pumiceous clasts. The higher density values correlate to a decreased vesicularity range for the scoriaceous clasts, 34.27-56.53%. These changes are reflected in Figure 3.3 as the scoriaceous clasts tend to fill in the density distributions between the lower and higher density modes, and overlaps in density value with some of the higher density pumiceous clasts. An occasional intermediate mode around 1.75 g/cm³ appears to be due to high abundance of scoriaceous clasts with this density value overlapping with microcrystalline clasts with the same density value. The high-density mode tends to occur around a value of 1.9-2.1 g/cm³. This density value is largely represented by microcrystalline clasts which are gradational to scoriaceous clast densities and vesicularity (Table 3.7).

Table 3.5 - Average values of bulk rock density and vesicularity for Pu‘u Wa‘awa‘a pumiceous clasts by stratigraphic unit.

Sample	<i>n</i>	<i>N</i> (number Pumice)	Frequency (fraction)	Average ρ (10^3 kg m^{-3})	ρ range	Average Vesicularity (% vol.)	Vesicularity Range
P_151	100	72	0.72	0.65	0.36 - 1.11	73.24	56.46 - 86.12
P_152	100	62	0.62	0.71	0.42 - 1.65	69.95	35.52 - 83.54
P_153	100	78	0.78	0.70	0.33 - 1.41	70.51	44.83 - 86.93
P_251	100	84	0.84	0.64	0.33 - 1.25	73.79	52.85 - 87.23
P_351	100	49	0.49	0.71	0.35 - 1.60	69.42	38.60 - 86.29
P_451	100	59	0.59	0.81	0.41 - 1.59	65.66	37.75 - 84.16
P_452	125	61	0.49	0.65	0.36 - 1.57	71.04	38.50 - 85.87
P_551	84	60	0.71	0.65	0.38 - 1.07	73.73	58.02 - 85.33
P_552	125	29	0.23	0.88	0.49 - 1.58	62.93	38.14 - 80.87
P_651	125	60	0.48	0.73	0.36 - 1.54	68.31	39.95 - 85.92
P_652	135	60	0.44	0.73	0.29 - 1.54	69.19	35.78 - 88.74

Table 3.6 - Average values of bulk rock density and vesicularity for Pu‘u Wa‘awa‘a scoriaceous, Sc, clasts by stratigraphic unit.

Sample	<i>n</i>	<i>N</i> (number Sc)	Frequency (fraction)	Average ρ (10^3 kg m^{-3})	ρ range	Average Vesicularity (% vol.)	Vesicularity Range
P_151	100	5	0.05	1.54	1.40 - 1.69	37.71	24.51 - 51.92
P_152	100	10	0.10	1.33	0.91 - 1.67	45.94	34.83 - 64.55
P_153	100	6	0.06	1.40	1.26 - 1.62	44.78	36.79 - 50.78
P_251	100	7	0.07	1.20	0.98 - 1.50	52.00	41.57 - 61.88
P_351	100	10	0.10	1.59	1.30 - 1.88	36.75	26.71 - 49.22
P_451	100	12	0.12	1.28	0.93 - 1.82	47.83	28.73 - 63.80
P_452	125	22	0.18	1.52	1.09 - 1.84	39.25	23.31 - 57.56
P_551	84	20	0.24	1.05	0.84 - 1.62	56.53	36.69 - 73.47
P_552	125	21	0.17	1.56	1.17 - 1.96	37.37	23.29 - 54.20
P_651	125	20	0.16	1.60	0.97 - 2.16	34.27	15.58 - 62.20
P_652	135	20	0.15	1.39	0.98 - 1.84	44.10	28.21 - 61.97

Table 3.7 - Average values of bulk rock density and vesicularity for Pu‘u Wa‘awa‘a microcrystalline, Mc, clasts by stratigraphic unit.

Sample	<i>n</i>	<i>N</i> (number Mc)	Frequency (fraction)	Average ρ (10^3 kg m^{-3})	ρ range	Average Vesicularity (% vol.)	Vesicularity Range
P_151	100	14	0.14	1.98	1.55 - 2.33	19.88	9.16 - 39.42
P_152	100	15	0.15	1.93	1.66 - 2.15	23.47	16.15 - 34.97
P_153	100	12	0.12	1.90	1.68 - 2.14	24.88	16.31 - 34.33
P_251	100	7	0.07	1.88	1.68 - 2.06	25.78	19.56 - 34.36
P_351	100	24	0.24	1.97	1.58 - 2.34	20.44	8.41 - 38.20
P_451	100	18	0.18	1.87	1.44 - 2.47	22.80	3.67 - 43.77
P_452	125	35	0.28	1.93	1.51 - 2.29	22.83	10.41 - 40.84
P_551	84	3	0.036	1.64	1.48 - 1.79	35.25	30.13 - 42.10
P_552	125	46	0.37	1.99	1.43 - 2.26	20.37	11.66 - 44.24
P_651	125	33	0.26	2.06	1.67 - 2.42	17.85	5.54 - 34.78
P_652	135	43	0.32	1.90	1.45 - 2.36	23.62	7.70 - 43.42

The microcrystalline clasts have a higher mean density range, 1.64-2.06g/cm³ than both the pumiceous and scoriaceous clasts. These high-density values correspond to very low mean vesicularity values in the range 17.85-35.23%. These results confirm that the pumiceous clasts are on average the least dense clasts, scoriaceous clasts intermediate, and microcrystalline clasts the densest. The opposite trend is true for vesicularity contents, e.g. pumiceous clasts have the highest average vesicularity values. Additionally, the mean density value range for the microcrystalline clasts is close to the intermediate and high-density modes across all units. This indicates that microcrystalline clasts help account for the intermediate and high-density modes.

Obsidian clasts have a mean density range of 1.72-2.15 g/cm³ and a mean vesicularity range of 14.04-32.92% (Table 3.8). Note that this mean density value range indicates that obsidian clasts commonly occur as a main component in the high-density mode. Combining the density ranges and frequencies for each subunit we can see that high mean density values correspond to an overall high abundance of dense clasts. Similarly, the subunits with the lowest mean density values also have the lowest abundances of dense clasts. The subunits with a high abundance of dense clasts tend to have more distinct bimodal distributions. This makes sense as one mode corresponds to less-dense clasts and one mode tends to correspond with overlap between density values for the more-dense clasts.

Table 3.8 - Average values of bulk rock density and vesicularity for Pu‘u Wa‘awa‘a obsidian, Ob, clasts by stratigraphic unit.

Sample	<i>n</i>	<i>N</i> (number Ob)	Frequency	Average ρ (10^3 kg m^{-3})	ρ range	Average Vesicularity (% vol.)	Vesicularity Range
P_151	100	8	0.08	2.00	1.70 - 2.32	19.64	9.23 - 33.68
P_152	100	13	0.13	2.04	1.73 - 2.35	18.32	8.24 - 32.56
P_153	100	4	0.04	2.13	1.89 - 2.28	15.84	11.1 - 26.23
P_251	100	2	0.02	2.01	1.83 - 2.22	19.54	13.35 - 26.82
P_351	100	16	0.16	2.05	1.75 - 2.39	18.54	6.70 - 31.62
P_451	100	10	0.10	2.15	1.80 - 2.41	14.04	6.05 - 29.51
P_452	125	6	0.05	2.03	1.85 - 2.29	19.50	10.60 - 27.75
P_551	84	1	0.012	1.72	-	32.94	-
P_552	125	26	0.21	2.11	1.75 - 2.41	15.31	5.78 - 31.62
P_651	125	8	0.06	2.04	1.58 - 2.24	18.40	12.48 - 38.34
P_652	135	12	0.09	1.98	1.66 - 2.31	20.51	9.87 - 35.12

3.2.3. XRF Whole-Rock Compositions

The obtained major elemental compositions are presented as weight percent oxides in Table 3.9. For the obtained samples we can see that our results were very similar to results previously obtained by Cousens *et al.*, 2003. Analyses in this study returned results generally in agreement with values obtained in previous studies for the Wa'awa'a Volcanics (Cousens *et al.*, 2003; Moore *et al.*, 1987). Differences in obtained compositions may be in part due to high LOI for the Cousens *et al.* (2003) study. Compositions from both Pu'u Wa'awa'a and Pu'u Anahulu plot in the trachyte region of the total alkalis classification scheme (Figure 3.5). Note that from Figure 3.5 we can see that the Pu'u Wa'awa'a compositions all plot as a cluster while the Pu'u Anahulu compositions cluster together as a slightly higher SiO₂ wt. % and slightly lower total alkalis wt. % than the Pu'u Wa'awa'a samples.

Additional variations in oxides weight percentages are plotted in SiO₂ variation diagrams in Figure 3.6. From these figures we can see that the oxides with the most similar weight percentages between both sampled units are CaO, Fe₂O₃, and P₂O₅. Weight percentage differences between the Pu'u Wa'awa'a and Pu'u Anahulu analyses are very minor and show values of overlap for several oxides (CaO, Fe₂O₃, K₂O and P₂O₅). The other oxides show larger differences in oxide compositions. Interestingly, the Pu'u Wa'awa'a analyses only have higher weight percentages for the alkali oxides (Na₂O and K₂O) and MnO compared to the Pu'u Anahulu analyses. The processes that are typically attributed with slight changes in magmatic compositions are fractional crystallization of the magma chamber and the mixing of two magmas of difference compositions. The feasibility of these two processes is evaluated in the context of the obtained results in the *Discussions* section.

Table 3.9 – Whole-rock compositions of selected Pu‘u Wa‘awa‘a clasts and Pu‘u Anahulu lava blocks.

Sample ID: <i>n</i> (majors)	Pu‘u Anahulu Trachyte Lava Flow									Pu‘u Wa‘awa‘a Trachyte Cone								
	PA-BK-1 (2)	PA-BK-2 (2)	PA-BK-3 (2)	PA-BK-4 (2)	PA-BK-5 (1)	PA-BK-6 (2)	PA-BK-7 (2)	PA-BK-8 (2)	PA-BK-9 (2)	PWW – BK-1 (2)	PWW – BK-2 (2)	PWW – BK-3 (2)	PWW – BK-4 (2)	PWW – BK-5 (2)	PWW – BK-6 (2)	PWW – BK-7 (2)	P-451-9 (2)	P-651-2 (1)
SiO ₂	62.44	62.88	63.41	62.28	63.02	62.57	62.73	62.67	62.76	62.53	62.30	62.54	62.51	62.35	62.89	62.53	62.31	62.90
TiO ₂	0.45	0.46	0.45	0.45	0.45	0.45	0.45	0.45	0.45	0.38	0.38	0.37	0.38	0.38	0.37	0.37	0.37	0.37
Al ₂ O ₃	17.86	17.88	17.75	17.67	18.00	18.21	17.90	18.04	18.06	17.43	17.26	17.34	17.34	17.38	17.47	17.37	17.37	17.48
Fe ₂ O ₃ ^{tot}	4.57	4.58	4.47	4.50	4.55	4.63	4.69	4.53	4.61	4.54	4.54	4.53	4.56	4.53	4.51	4.56	4.49	4.50
MnO	0.26	0.22	0.18	0.27	0.23	0.26	0.27	0.26	0.23	0.30	0.30	0.31	0.30	0.30	0.30	0.31	0.31	0.30
MgO	0.57	0.55	0.49	0.60	0.50	0.54	0.53	0.55	0.51	0.49	0.47	0.48	0.47	0.49	0.48	0.46	0.47	0.49
CaO	0.94	0.91	0.87	0.97	0.88	0.78	0.86	0.89	0.90	0.90	0.89	0.88	0.89	0.88	0.88	0.88	0.89	0.89
Na ₂ O	7.10	6.92	6.67	7.13	6.94	6.86	7.02	6.87	6.82	8.06	7.64	7.92	7.78	8.05	7.94	7.54	7.99	7.88
K ₂ O	4.83	4.92	4.84	4.86	4.92	4.92	4.89	4.87	4.92	4.97	4.98	4.96	4.97	4.94	4.98	4.98	4.98	4.97
P ₂ O ₅	0.19	0.18	0.19	0.21	0.18	0.06	0.17	0.17	0.18	0.17	0.17	0.17	0.16	0.18	0.17	0.15	0.15	0.15
SUM	99.21	99.50	99.32	98.94	99.69	99.28	99.51	99.30	99.44	99.77	98.93	99.50	99.36	99.48	99.99	99.15	99.33	99.93

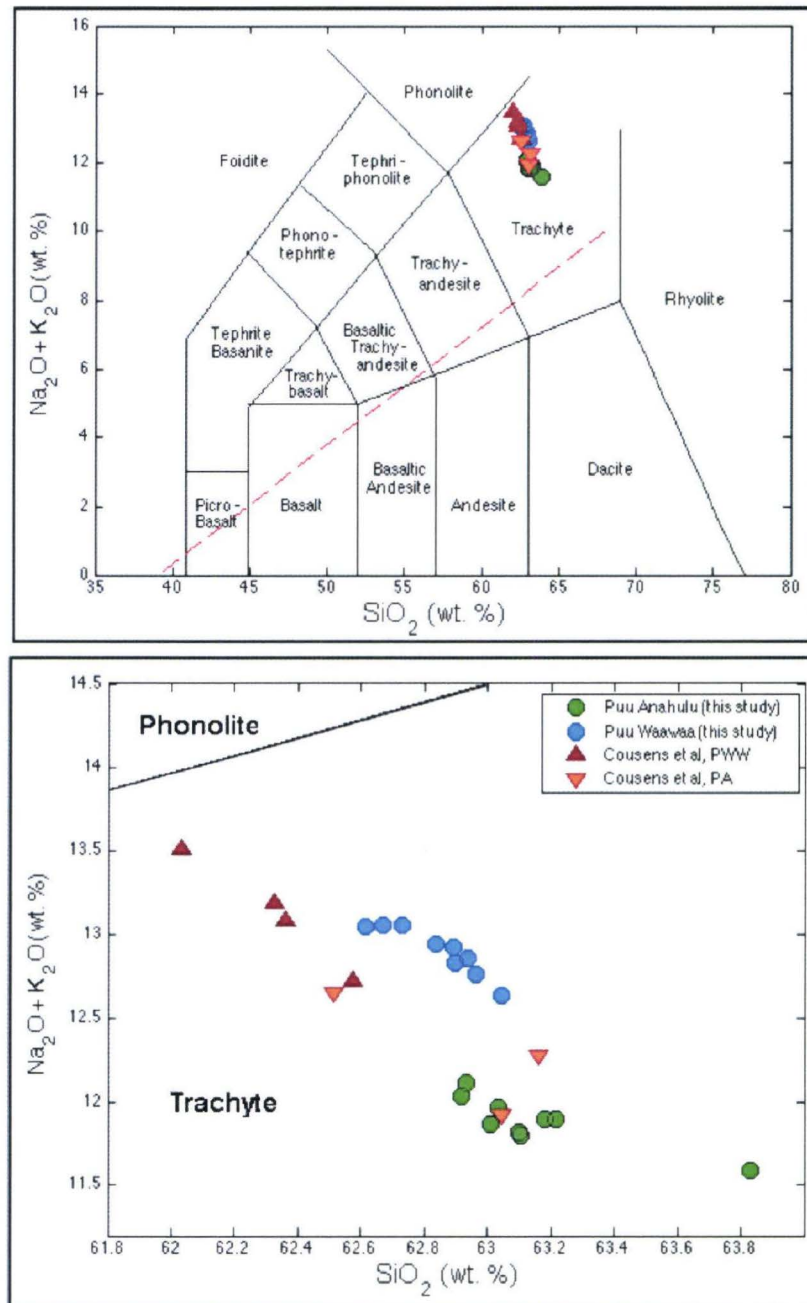


Figure 3.5 - (Top) Total alkalis versus silica diagram showing the Pu'u Wa'awa'a and Pu'u Anahulu compositions in the context of the Total Alkalis Classification scheme (derived from *Le Bas et al.*, 1986). (Bottom) Highlights the slightly more alkali nature of the Pu'u Wa'awa'a trachyte.

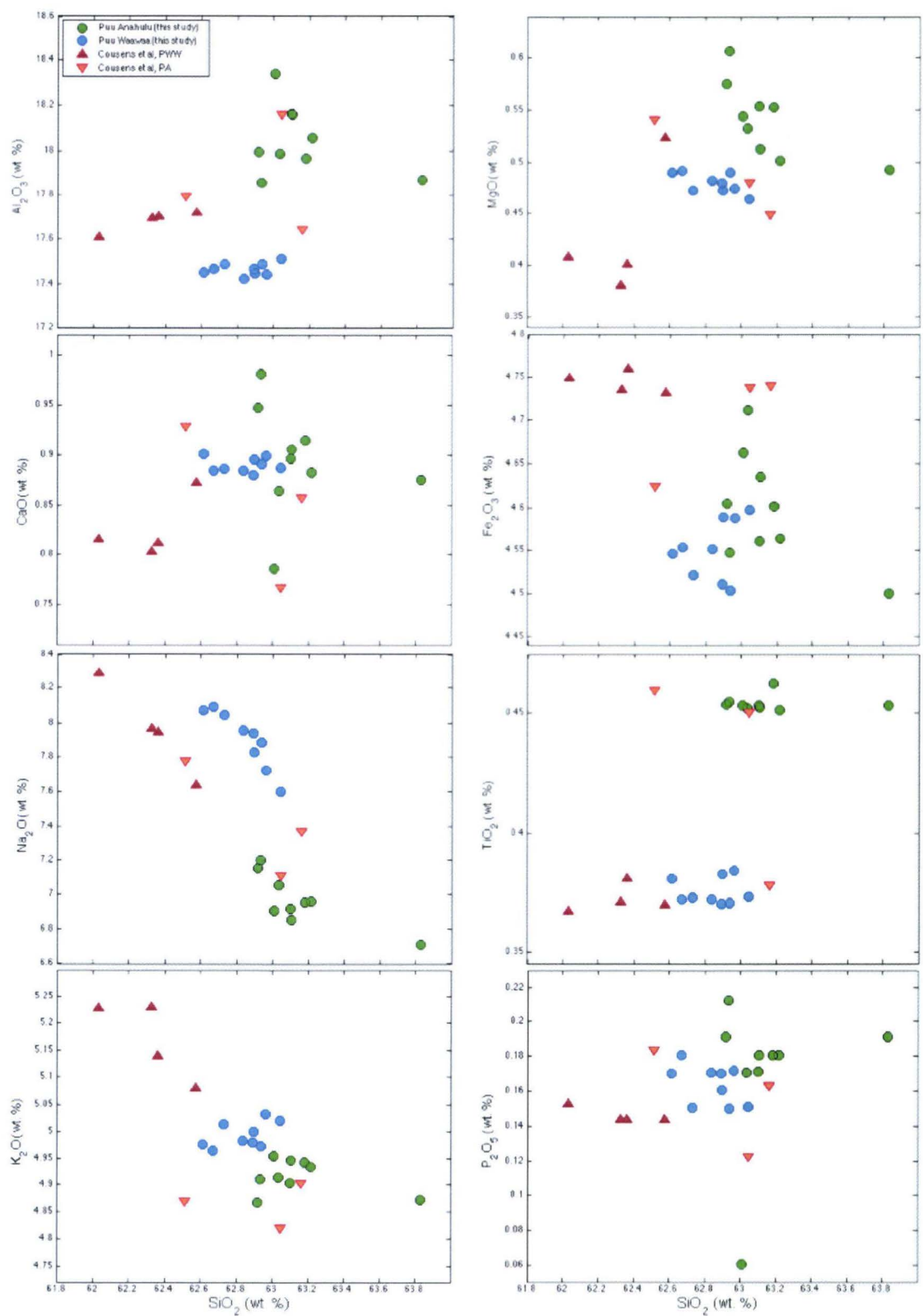


Fig. 3.6 - Whole-rock SiO_2 variation diagrams.

CHAPTER 4.

DISCUSSION

4.1. ACCOUNTING FOR TEXTURAL DIVERSITY THROUGH ERUPTION STYLE

The relatively small volume of ejecta material, $\sim 0.5\text{km}^3$ for the trachyte cone in total (Moore *et al.*, 1987), is representative of the volume of material typically ejected in vulcanian explosions, which is on the order of 0.1km^3 (Morrissey and Mastin, 2000). As the Pu‘u Wa‘awa‘a cone consists of multiple eruption packets as noted by bimodal density distributions, clast frequency variability, and discrete eruption deposit packets (this study) we can assume that the volume of each eruption resulting in a deposit was less than 0.5km^3 and thus closely approximates volumes expected for vulcanian explosions. These features of relatively short duration and small volume deposits present at Pu‘u Wa‘awa‘a are features characteristic of vulcanian explosions (Self *et al.*, 1979; Sparks *et al.*, 1997; Stix *et al.*, 1997; Morrissey and Mastin, 2000).

Important to note from the results obtained in this study is the presence of a variety of textural components. The types of clasts within a volcanic deposit are useful indicators of the processes resulting in the eruption of the pyroclastic material and the eruption style. The wide variety of clasts erupted at Pu‘u Wa‘awa‘a (e.g. pumiceous clasts, scoriaceous clasts, glassy obsidian clasts and microcrystalline clasts) is in accordance with the wide range of components observed in Vulcanian eruptions (Morrissey and Mastin, 2000; Clarke, 2013). While obsidian clasts have been observed in plinian to sub-plinian deposits as well (Rust and Cashman, 2007), these eruptions tend to lack the range of textural variety observed in this study.

Additionally, the density distributions in the sampled units show a tendency to be bimodal. These bimodal density distributions vary from what is expected for plinian to sub-plinian eruptions and instead more closely resemble the bimodal distributions obtained for vulcanian explosions (Hoblitt and Harmon, 1993; Giachetti *et al.*, 2010).

Coupling these observations with the intermediate trachytic composition of Pu'u Wa'awa'a and the variety of textural classes accurately explained by the range of textures documented for vulcanian explosions (Formenti and Druitt, 2003; Clarke *et al.*, 2007; Burgisser *et al.*, 2010), we interpret the collected data to indicate the formation of Pu'u Wa'awa'a trachyte cone through vulcanian explosions.

There have been several studies on the formation of a conduit plug that facilitates magma degassing, fragments when overpressure in the conduit reaches a critical value, and erupts the magma in the volcanic conduit (Giachetti *et al.*, 2010 and references therein). We believe the cyclic formation of conduit plugs and their subsequent eruption led to the stratigraphic succession observed at Pu'u Wa'awa'a tephra cone. These results also bear striking resemblance to the data obtained on Monte Nuovo in the Phlegrean Fields, Italy in terms of componentry, deposit characteristics and physical conditions of the eruption products (D'Oriano *et al.* 2005; Piochi *et al.*, 2005). Due to the lack of first-hand information concerning Pu'u Wa'awa'a eruption, we correlated our data with observations from vulcanian explosions with similar compositions and deposit features to explain the processes at work at Pu'u Wa'awa'a.

4.2. ERUPTION MODEL FOR THE WA'AWA'A VOLCANICS

Combining pre-existing knowledge of the processes and dynamics at work during Vulcanian eruptions we developed a conceptual model for the eruption of Pu'u Wa'awa'a

trachyte cone modified from previously developed models for this style of eruption (Giachetti *et al.*, 2010; Burgisser *et al.*, 2010). Magma of a homogeneous composition follows a slow viscous ascent from the magma chamber up the volcanic conduit. As the magma rises, the pressure from overlying rocks decreases, allowing for the decompression of the magma and initiation of a suite of processes leading to the formation of a conduit plug and its subsequent eruption (Sparks, 1997; Barmin *et al.*, 2002; Melnik and Sparks, 2002; Giachetti *et al.*, 2010). A summary of the eruption model is given in Figure 4.1.

The initial slow viscous ascent of magma into the conduit allows for the decompression of magma and nucleation of volatile species, potentially H₂O in this case (as evidenced by preliminary FTIR analyses). As the magma rises, new vesicles continue to nucleate and pre-nucleated vesicles grow in size. This exsolution of volatile species results in a decrease in the amount of H₂O in the melt, thus raising the liquidus temperature of the rock (Hammer and Rutherford, 2002). The increase in liquidus temperature allows for nucleation of anhydrous phases, feldspar in this study. As the magma rises, vesicles continue to nucleate and grow and eventually start to coalesce as more volume is occupied by gaseous phases (Gonnermann and Manga, 2007 and references therein).

At this point the melt is relatively depleted in volatile species and nucleated crystals grow in size due to cooling at slower rates, this increases the degree of undercooling (necessary for crystal nucleation and growth) and allows for crystal growth (Sparks and Pinkerton, 1978; Swanson *et al.*, 1989; Spieler *et al.*, 2004b). As the number of crystals present increases, the vesicles become more crowded and pinched

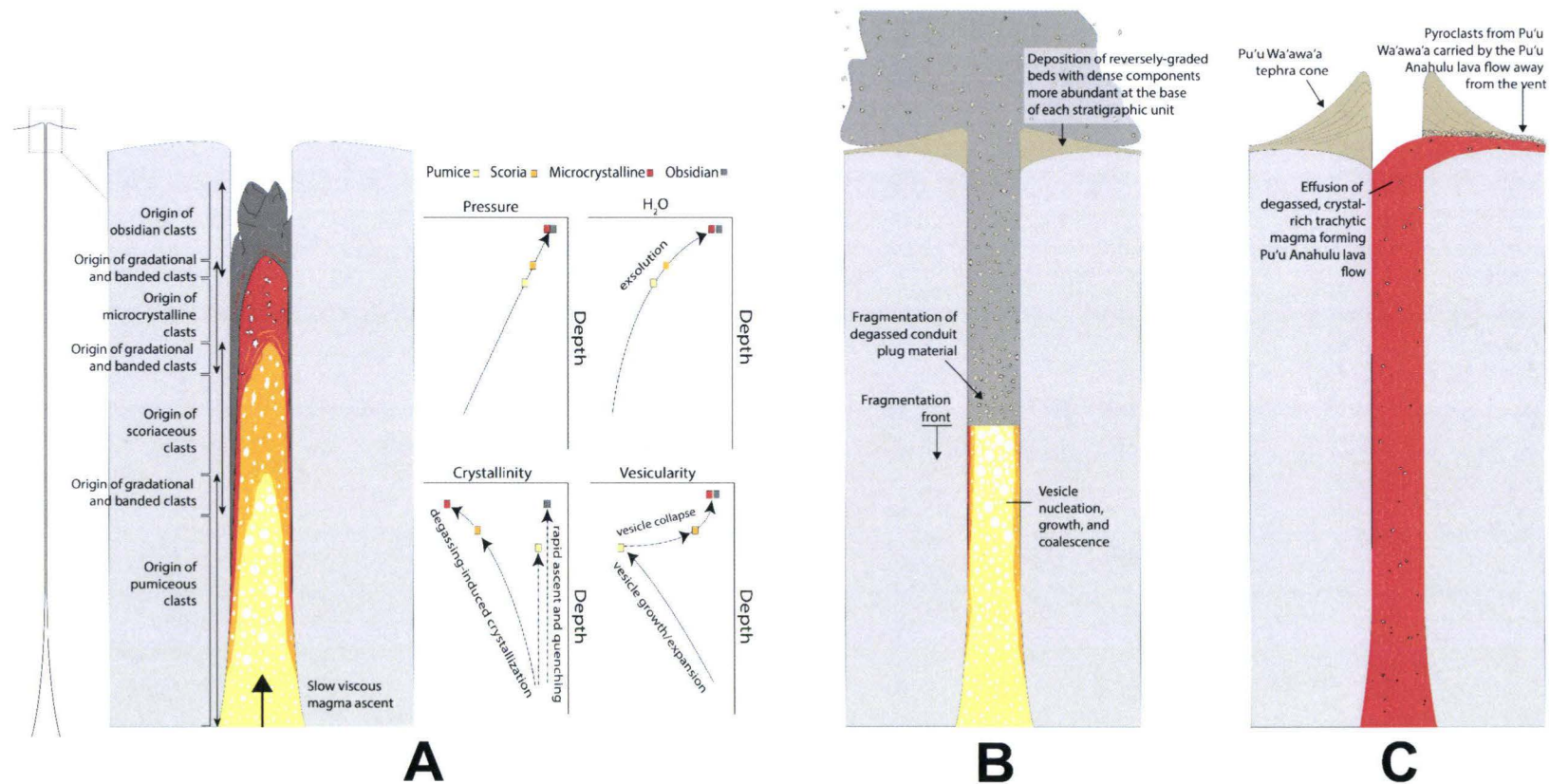


Figure 4.1 – Summary of vesiculation and crystallization processes during each Vulcanian explosion at Pu'u Wa'awa'a and during the effusion of Pu'u Anahulu.

with boundary expansion limited by crystals, which in turn obtrude on vesicle walls. Larger vesicles form chains in the magma allowing for escaping of volatile phases through degassing out the top of the plug and to surrounding country rock (Stasiuk *et al.*, 1996; Melnik and Sparks, 1999; Tuffen *et al.*, 2003; Gonnermann and Manga, 2003). Portions of the conduit that have undergone degassing retain a high crystallinity and low vesicularity if cooling of the magma is slow enough to allow for crystals to form or retain a glassy texture if cooling is too fast to allow for crystallization of the melt.

Evaluating this model in the context of results obtained in this study we inferred how the magma in the volcanic conduit cooled such that obtained physical results were explained through the degassing, vesiculation, and crystallization history of the magma.

Following initial injection of magma into the volcanic conduit, degassed material along the surfaces of the conduit cooled rapidly as it came into contact with surrounding much cooler country rock producing the glassy, crystal-poor component (obsidian). The vesicles in these samples are very small and rounded which was interpreted as a return to the rounded shape of initially nucleated vesicles. These obsidian clasts are commonly banded with crystal-rich, vesicle-poor microcrystalline material (Figure 3.1.D). The banding between degassed crystal-poor and degassed crystal-rich material is interpreted as the product of thermal mingling of the two components (Seaman, 1995; Perugini *et al.*, 2004).

The next region towards the center of the conduit plug cools slower than the rapidly quenched outermost layer and is presumed to correspond to the microcrystalline textural component. In this region magma slowly degasses through channels of preferred flow characterized by high permeability (Eichelberger *et al.*, 1986; Giachetti *et al.*, 2010).

Petrographically, these channels are distinguished by the presence of large vesicles aligned in chains that have been proposed to have previously been connected (Giachetti, *et al.*, 2010). The few remaining vesicles are irregular and collapsed in morphology due to a high number of crystals obtruding their walls. This region produces microcrystalline material that grades into scoriaceous material as you move away from the surfaces of the conduit.

The next region towards the center of the conduit cools slower than the microcrystalline material region. This allows for continued mobility of volatile phases and growth of crystals. However, as this material stays warmer longer, a smaller number of crystals grow before the conduit plug' eruption. This is due to the smaller degree of undercooling attained over a given time by a reduced cooling rate. From microcrystalline to scoriaceous regions we see an increase in vesicularity, which accounts for the variability in measured clast densities, and decrease in crystal content. The scoriaceous material grades into a more vesicle-rich and crystal-poor region of pumiceous material at the center of the conduit.

The center of the conduit is composed of pumiceous material that undergoes vesicle nucleation and growth as the magma rises. The nucleation and growth of vesicles continuously removes volatile species from the melt, causing an increasing liquidus temperature, and making undercooling a difficult, if not impossible, task in this region. We attribute the formation of very few crystals in this region to the inability of the melt to attain a high degree of undercooling. As volatile species in the center of the conduit exsolve, vesicles form and degas through the surrounding regions through channels of preferential degassing. Eventually, as the magma cools it passes through the glass

transition temperature range causing a shift from ductile to brittle deformation of the magma (Dingwell, 1996; Sparks, 1997). Combining this physical transition with the increased crystal content of the magma, vesicles can no longer degas through the magma as the viscosity of the magma becomes too great to allow vesicle mobility, called rheological stiffening (Sparks, 1997; Melnik and Sparks, 1999; Massol and Jaupart, 1999; Barmin *et al.*, 2002; Clarke, 2013). This entrapment of vesicles within the conduit increases volatile pressures and causes the conduit to become over-pressurized (Sparks, 1997; Massol and Jaupart, 1999; Clarke, 2013). When a critical over-pressurization threshold is reached, on the order of MPa's (Burgisser *et al.*, 2010), the conduit plug ruptures.

Rupturing of the conduit plug causes rapid decompression and consequent rapid expansion of vesicles in the conduit, which in turn leads to the acceleration, fragmentation and eruption of the material in the volcanic conduit (Melnik and Sparks, 2002; Mason *et al.*, 2006). Rupture also generates a rarefaction wave propagating down the eruption column, which is followed by the downward propagation of the fragmentation front (Melnik and Sparks, 2002). The downward propagation of the fragmentation front is supported by reverse-grading observed in each stratigraphic unit (D'Oriano *et al.*, 2005). In each stratigraphic unit, lighter colored, more vesicle-rich, pyroclasts increase in abundance from base to top of each unit and denser, more vesicle-poor and crystal-rich, pyroclasts decrease in abundance from base to top of the unit. This makes sense as we would expect the top of the erupted conduit plug to contain more dense material than material erupted from greater depth.